THE JOURNAL OF PHYSICAL CHEMISTRY B

Article

pubs.acs.org/JPCB

Kinetic Modeling of Hydrogen Conversion at [Fe] Hydrogenase Active-Site Models

Arndt R. Finkelmann, Martin T. Stiebritz, and Markus Reiher*

Laboratorium für Physikalische Chemie, ETH Zurich, Wolfgang-Pauli-Str. 10, 8093 Zurich, Switzerland

ABSTRACT: By means of density functional theory, we investigate the catalytic cycle of active-site model complexes of [Fe] hydrogenase and study how ligand substitutions in the first coordination sphere of the reactive Fe center affect the free-energy surface of the whole reaction pathway. Interestingly, dispersion interactions between the active site and the hydride acceptor MPT render the hydride transfer step less endergonic and lower its barrier. Substitution of CO by CN^-, which resembles [FeFe] hydrogenase-like coordination, inverts the elementary steps H^- transfer and H_2 cleavage. A simplified kinetic model reveals the specifics of the interplay between active-site composition and catalysis. Apparently, the catalytic efficiency of [Fe] hydrogenase can be attributed to a flat energy profile throughout the catalytic cycle. Intermediates that are too stable, as they occur, e.g., when one CO ligand is substituted by CN^-, significantly slow down the turnover rate of the enzyme. The catalytic activity of the wild-type form of the active-site model could, however, be enhanced by a PH_3 ligand substitution of the CO ligand.

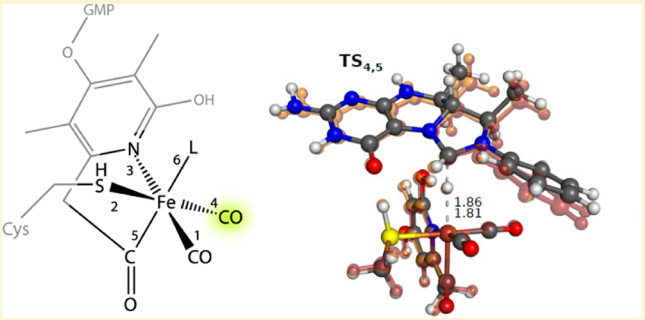

1. INTRODUCTION

Hydrogenases catalyze the reversible oxidation of H_2. Three evolutionary unrelated classes of hydrogenases exist.[1−4] [FeFe] hydrogenases and [NiFe] hydrogenases, which catalyze the reaction, $H_2 \rightleftharpoons 2\ H^+ + 2\ e^-$, differ in their catalytic preferences. Whereas [FeFe] hydrogenases are the most efficient H_2 producers, [NiFe] hydrogenases are better catalysts for the oxidation of H_2.[5] In sharp contrast, [Fe] hydrogenase catalyzes the heterolytic cleavage of H_2 with methenyltetrahydromethanopterin (MPT^+) as hydride acceptor which is reduced to methylenetetrahydromethanopterin (HMPT, see Figure 1).[6−9]

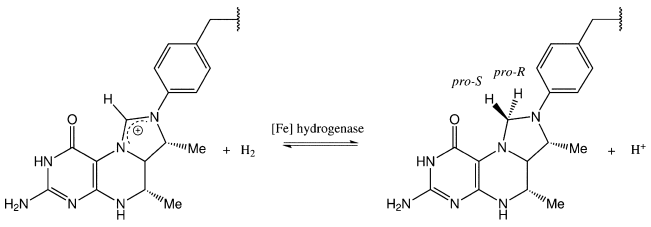

Figure 1. Reaction catalyzed by [Fe] hydrogenase.

Upon H_2 splitting the hydride is stereospecifically transferred to the *pro-R* position of C14a of MPT^+ as deduced from NMR experiments.[10,11] This reaction is slightly exergonic by −1.3 kcal/mol.[12]

Unfortunately, all variants which are efficient in the H_2-producing reaction regime (as opposed to H_2 oxidation), like [FeFe] hydrogenases and certain [NiFe] hydrogenases, are reversibly or irreversibly inhibited by O_2 (see ref 13 for a review of experimental and theoretical results and refs 14−17 for quantum chemical results on the molecular mechanism of oxygen inhibition of [FeFe] hydrogenase and iron−sulfur clusters). This problem represents a severe drawback for their technical application. The H_2-splitting [Fe] hydrogenase, however, is stable against molecular oxygen as triplet O_2 does not bind to its active site.[18,19] The active sites of [FeFe] and [Fe] hydrogenases share similarities in the first-shell coordination sphere. A prominent difference is the two CO ligands in the basal plane of the octahedron in the active site of [Fe] hydrogenase opposed to a CO, CN^- arrangement in [FeFe] hydrogenases (CO and CN^- ligands also occur in the active site of [NiFe] hydrogenases). Quantum chemical studies show that the thermodynamics of O_2 coordination to the active sites of [FeFe] and [Fe] hydrogenases is sensitive with respect to the ligands in the coordination spheres of the reactive Fe centers.[19,20] However, with respect to the regular catalytic activities of these enzymes, the question about the significance of the particular ligand choices in both active sites arises. This point can only be addressed by detailed kinetic modeling of the catalytic cycles. [Fe] hydrogenase appears to be a perfect target for such a kinetic study of first-shell ligand effects for its active site contains only a single (active) metal center, while the reactive centers of other hydrogenases are composed of polynuclear transition-metal clusters. Reactivity principles discovered in the course of such a study may eventually be transferred to mononuclear biomimetic model complexes. They

Received: December 21, 2012
Revised: April 5, 2013
Published: April 5, 2013

dx.doi.org/10.1021/jp312662y | *J. Phys. Chem. B* 2013, 117, 4806−4817

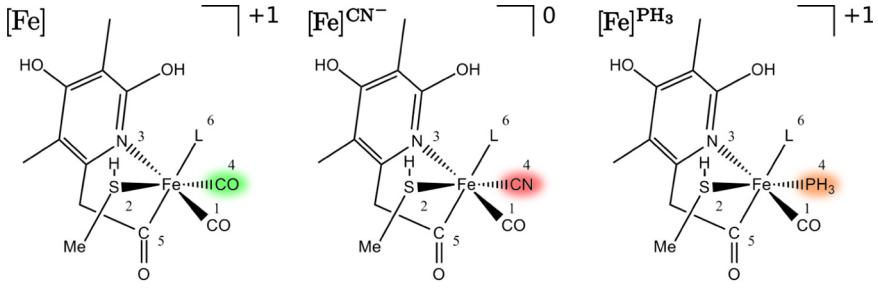

Figure 2. Lewis models of the three variants [Fe], $[Fe]^{CN^-}$, and $[Fe]^{PH_3}$. The ligand in position 4 is shown in color.

proved to be very successful for understanding the structure and function of the active sites of hydrogenases.[21] A striking example is the nickel based hydrogen evolving catalyst of DuBois and co-workers[22,23] which is inspired by the active site of [FeFe] hydrogenases. The field of [Fe] hydrogenase model complexes has been growing recently, since the active-site structure of the enzyme was elucidated by X-ray crystallography. Many structural active-site models have been synthesized and characterized, which helped to understand structural and spectroscopic features of the naturally occurring form.[24−35]

The crystal structure of the iron-guanylylpyridinol (FeGP) containing enzyme from *Methanocaldococcus jannaschii* was first determined by Shima et al.[36] Improved refinement of a mutant protein (C176A) revealed an apical acyl group bound to a pyridinol moiety as a ligand.[37] At first glance, the active sites of [Fe] and [FeFe] hydrogenases appear to be quite different, but closer inspection, however, reveals a striking similarity in the first-shell coordination spheres of the catalytically active Fe atoms.[20]

In this work, we investigate changes in the catalytic mechanism of an active-site model of [Fe] hydrogenase by small modifications of the first ligand shell. The construction of active-site variants is motivated by the principle of swapped first-shell ligand spheres.[20] We focus on the ligand in position four due to its dominating impact on O_2 affinity.[19] Exchange of CO by CN^- leads to a [FeFe]-like variant dubbed $[Fe]^{CN^-}$. In addition, we choose a form with phosphine in position four (dubbed $[Fe]^{PH_3}$) in order to study the influence of a weak-field ligand and strong σ-donor (PH_3) compared to the π-acceptors CO and CN^-. Phosphorus-based ligands have already been employed in biomimetic hydrogenase complexes (see, e.g., refs 30, 33, and 38) and even a model complex with a phosphorus ligand trans to a thiolate ligand exists.[27] Lewis structures of the wild-type model and the two variants studied in this work are depicted in Figure 2. It should be clear that the mechanistic results obtained for these three models derived from the active-site structure of [Fe] hydrogenase are important for the rational design of structural and functional biomimetic model complexes.

We begin this investigation by studying the regular catalytic mechanism of H_2 splitting at the active site of [Fe] hydrogenase based on the pioneering work published by Yang and Hall[39] and explore the effect of single ligand exchanges on both thermodynamics and kinetics of each reaction step. We focus on reactivity changes of the isolated reaction center embedded into a dielectric continuum to model the protein environment. It is crucial to separate first-shell ligand effects from modifications introduced by the protein matrix in order to uncover the generic reactivity of the cluster. The mechanism for the reaction catalyzed by [Fe] hydrogenase (compare Figure 1) comprises two crucial steps: Hydrogen cleavage at the iron center and hydride transfer to the cosubstrate MPT^+. For the Hall mechanism,[39] we elucidate the energetics of the different variants taking also dispersion interactions into account. After having revisited the Hall mechanism, we construct two variants of the FeGP cofactor and assess the influence of the different first-shell ligands on the catalytic cycle. Based on these results a kinetic model is developed that allows the correlation between first-shell substitutions and catalytic efficiency to be understood.

2. COMPUTATIONAL METHODOLOGY

The starting structures for structure optimizations were taken from ref 39 with one exception discussed below. The ligand variants were constructed by replacement of the ligands and adjustment of the overall molecular charge. Density functional theory (DFT) was applied with the BP86 and TPSS exchange-correlation functionals,[40−42] a triple-ζ def-TZVP basis set,[43] and empirical dispersion corrections (DFT-D3)[44] as implemented in the Turbomole program package.[45] The methodology was evaluated by testing different functionals with and without dispersion correction. Advantage was taken of the resolution-of-the-identity approximation (RI) with the corresponding auxiliary basis sets.[46] For the reaction mechanism all structures were optimized as isolated systems. Stable intermediates and transition states were confirmed by vibrational analysis. On the optimized structures single-point calculations with the polarizable continuum model COSMO[47] with a modified radius for iron, as suggested in ref 48, were performed. A dielectric constant of $\varepsilon = 4$ was chosen to account for the screening effect of the protein matrix (see, e.g., ref 49). Thermodynamic quantities were calculated by approximating the translational, rotational and vibrational degrees of freedom by the ideal gas, rigid rotor, and harmonic oscillator models.

Wavenumbers obtained with the BP86 density functional are scaled by a factor of 0.9914 according to ref 50 for the calculation of zero-point vibrational energies and Gibbs free energies. Note that Gibbs free energies for reaction steps that differ in the number of educt and product molecules have to be considered with care due to the applied ideal gas assumption which is a poor approximation for obtaining translational degrees of freedom in condensed phases. In these cases Gibbs free energies are erroneous by about 10 kcal/mol (see, e.g., ref 51).

The reaction mechanism comprises a deprotonation step. To estimate the free energy for this step we need to know the free energy of solvation for the proton. There is an ambiguity regarding this quantity in the literature. Experimentally obtained and theoretically derived values range from −252.6 to −262.5 kcal/mol.[52] We chose to take a $\Delta G_{solv,H^+} = -262.4$

dx.doi.org/10.1021/jp312662y | J. Phys. Chem. B 2013, 117, 4806−4817

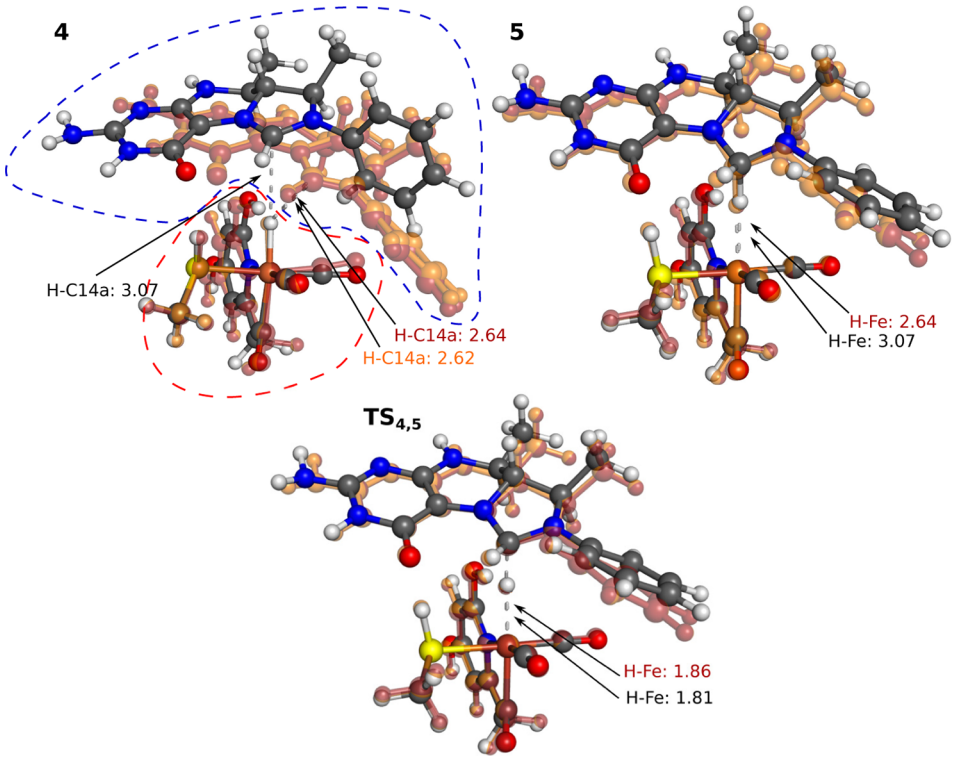

Figure 3. Superposition of optimized structures for intermediates **4** and **5** and transition state $\mathbf{TS}_{4,5}$. The foreground structures are the structures from Yang and Hall[39] obtained with TPSS. The pale red structures are obtained with BP86-D3, the pale orange structures with TPSS-D3. The C14a–H^- and Fe–H^- bond lengths are given in Ångstroms and are colored according to the corresponding structure. Dotted red and blue lines indicate regions one and two for the calculation of the pairwise dispersion interaction energies (compare also Table 1). Color code: C, gray; Fe, brown; H, white; N, blue; O, red; S, yellow.

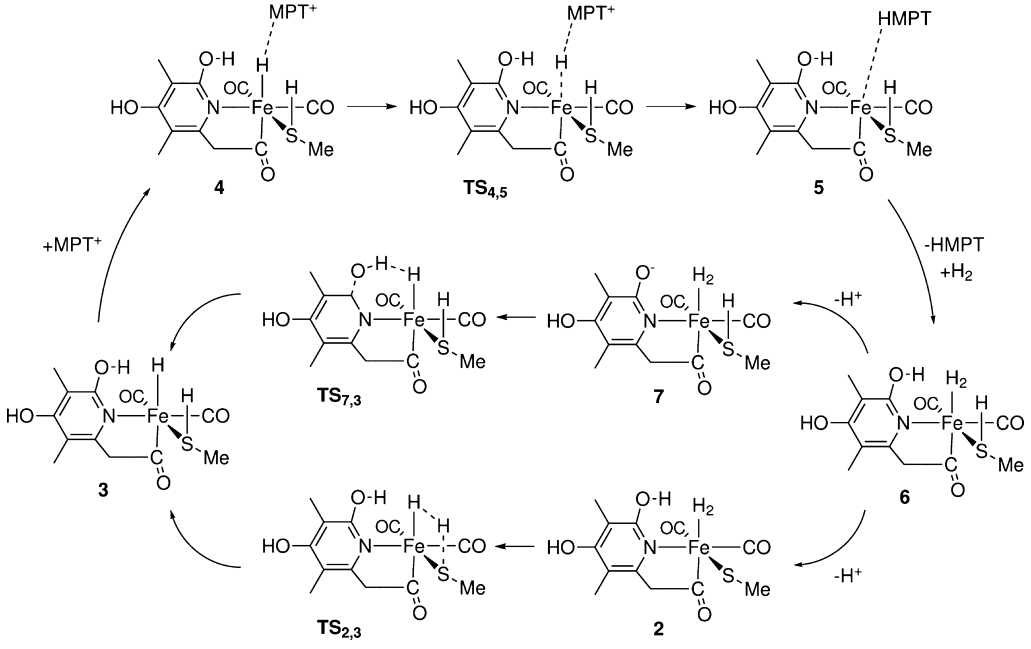

Figure 4. Reaction mechanism proposed by Yang and Hall.[39]

kcal/mol which is based on gas-phase hydration data[53] and is also in accordance with theoretical predictions.[52]

Furthermore, the reaction cycle of [Fe] hydrogenase involves binding and dissociation of the cosubstrate MPT^+/HMPT (steps **3** → **4** and **5** → **6** in Figure 4) for which our model cannot account for. Within the protein framework binding of $HMPT^+$ and successive cleavage are processes which can be expected to underlie a subtle control by the protein surrounding. Thus, a simple description by differences in free energies of coordinated and uncoordinated isolated complexes is a rather crude approximation to the process that actually happens in the enzyme. This problem can be overcome by

dx.doi.org/10.1021/jp312662y | J. Phys. Chem. B 2013, 117, 4806–4817

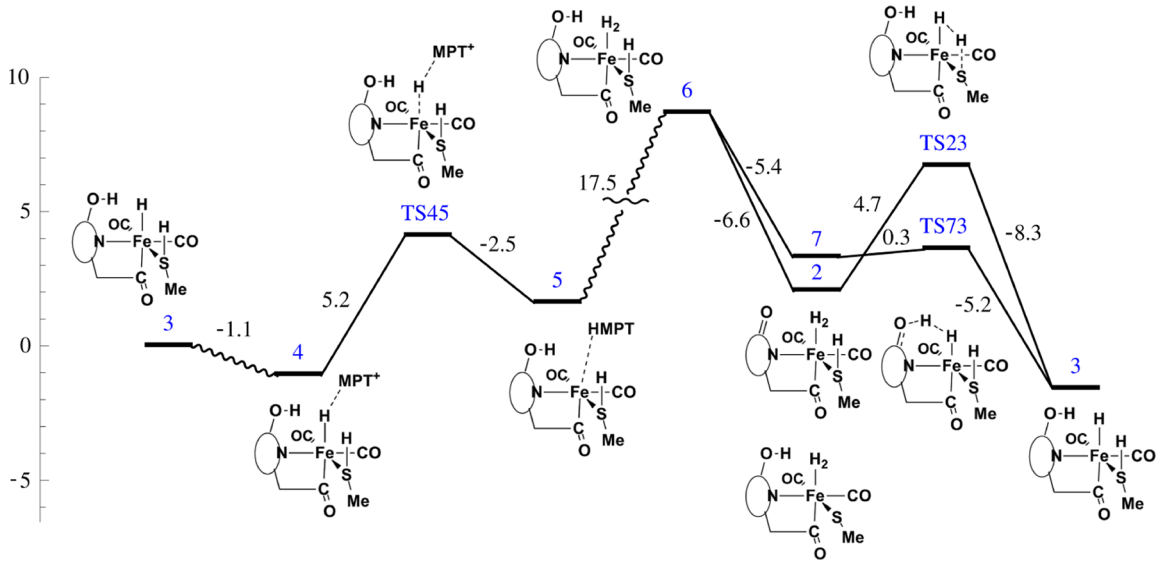

Figure 5. Free-energy profile calculated with BP86-D3/TZVP/COSMO (ε = 4). Gibbs free energies are given in kcal/mol (T = 298 K, p = 1.013 bar). The wiggly lines indicate that the difference in free energy is not representative for the reaction in the enzyme as interactions of the cofactor with the protein matrix are not considered here.

calibrating these energies to the total free energy of the catalytic cycle[39] which is stated to be −1.3 kcal/mol.[12] This is, however, not suited for the comparison of different variants of the active site that we shall present here. We therefore provide the calculated energies of the above-mentioned reaction steps but indicate that these are not representative for the process in the enzyme by wiggly lines in Figures 5, 7, and 8. Yang and Hall discussed that deprotonation of the cysteine residue can also occur from intermediate **4** before the hydride is transferred, leading to an alternative pathway.[39] The resulting deprotonated structure of intermediate **4** is, however, not a stable minimum on the potential energy surface obtained with our methodology. Therefore, the resulting pathway will not be discussed here.

For intermediate **4** we did not take the structure from ref 39 as starting point for our optimizations as it is not the proper educt corresponding to the transition state within our ansatz. Our structure for intermediate **4** was obtained by distorting the structure of $\mathbf{TS}_{4,5}$ along the normal mode corresponding to the imaginary frequency and subsequent structure optimization. The difference between our structure and the one described in ref 39 is depicted in Figure 3.

There appears to be another small inconsistency with intermediate **3** concerning the position of the hydrogen atom connected to the cysteine's sulfur atom (H^S) in ref 39. Inspection of the H^S−S−Fe−H dihedral angle H^S shows that the hydrogen atom is oriented toward the CO ligands, hence, away from the pyridinol ligand. In $\mathbf{TS}_{2,3}$ and, very clearly, in $\mathbf{TS}_{7,3}$ H^S is oriented toward the pyridinol ligand, forming a hydrogen bridge in $\mathbf{TS}_{7,3}$. Therefore, intermediate **3** as reported Yang and Hall is not the product corresponding to the transition state. The rotational barrier for this bond can be considered small, thus the interpretations are not affected. Figures of molecular structures were created with ChemDraw[54] and PyMOL.[55]

3. RESULTS

3.1. Hall Mechanism Revisited. In order to investigate the effect of ligand substitutions on the catalytic activity of [Fe] hydrogenase, it is imperative to first study the mechanism facilitated by the native active site. From explorative calculations we realized that central steps in this process are altered if dispersion interactions are considered explicitly. For this reason we briefly review the Hall mechanism[39] which was established without taking dispersion interactions into account, followed by reporting the changes due to such interactions. The mechanism for the catalytic reduction of MPT^+ with H_2 to form HMPT and H^+ proposed by Yang and Hall[39] is shown in Figure 4. After a coordinating water molecule in position 6 is replaced by H_2, the cycle starts at intermediate **6**. To be able to cleave H_2 the complex first has to be deprotonated which can either occur at the cysteine ligand (step **6** → **2**) or at the hydroxyl group of the pyridinol ligand to give intermediate **7** (step **6** → **7**). The deprotonation of the hydroxyl group is favored by 2 kcal/mol, according to Yang and Hall.[39] Both possibilities result in the formation of a proton acceptor thereby facilitating subsequent H_2 cleavage. H_2 cleavage is exergonic by −3.4 (−1.2) kcal/mol and has a barrier of 6.6 (3.3) kcal/mol for reaction **2** → **3** (and reaction **7** → **3**). The binding of MPT^+ triggers hydride transfer from Fe to the cosubstrate (formation of HMPT). This reaction is endergonic by 9.9 kcal/mol and has a barrier of 15.2 kcal/mol and can, consequently, be considered as the rate determining step, as reported in ref 39. All energies reported by Yang and Hall[39] correspond to structure optimizations with the TPSS exchange-correlation functional followed by single point calculations with the integral equation formalism polarizable continuum model (IEFPCM) and a dielectric constant of ε = 4.

The reaction profile obtained with the explicit treatment of dispersion interactions and the BP86 exchange-correlation functional is shown in Figure 5. The most prominent change, compared to the one by Yang and Hall, is that the energetics of the rate determining hydride transfer step is significantly changed. Product formation is now endothermic by +2.7 kcal/mol (BP86-D3) as opposed to +10.9 kcal/mol (TPSS) and the barrier height is reduced from +15.2 kcal/mol (TPSS) to +5.2 kcal/mol (BP86-D3). Consequently, this reaction should be fast under physiological conditions. The question is how dispersion interactions cause these energetic changes. Compar-

dx.doi.org/10.1021/jp312662y | J. Phys. Chem. B 2013, 117, 4806−4817

ing the optimized structures shows that the relative position of the cosubstrate and the active site change if dispersion interactions are considered (see Figure 3). For intermediate **4** MPT^+ lies significantly closer to the Fe atom and the distance between the hydride species and the hydride accepting carbon atom (C14a) of MPT^+ is only 2.64 Å compared to 3.07 Å in the reference structure given by Yang and Hall (TPSS/6-31++G(d,p)). Structures obtained with TPSS-D3 have a similar hydride−C14a distance like those obtained with BP86-D3, indicating that the shortening of this distance is solely due to dispersion corrections. Apparently, dispersion-induced structural differences are more prominent for intermediate **4** than for transition state $\mathbf{TS}_{4,5}$ and product **5** (see Figure 3).

Based on manipulations of the crystal structure (fitting the open conformation of a mutated holoenzyme to closed conformation of the apoenzyme) Hiromoto et al.[56] concluded that the Fe−C14a distance is about 3 Å. We take this even shorter distance as an indication that close spatial proximity of FeGP and MPT^+ might also be imposed by the protein which supports our results.

Due to the different relative positioning of MPT^+ and FeGP it might also be possible that the pairwise dispersion energy between these two fragments changes during the course of the reaction. To analyze this effect, the complex is divided into two regions as indicated in Figure 3. Region one is the cofactor (truncated model of FeGP), region two is MPT^+. It can be seen that a significant contribution of the pairwise interaction energies stems from interactions between both regions. The sum of these energies (total dispersion energy) only increases by 0.9 kcal/mol during the course of the reaction. The product is stabilized by additional 2.0 kcal/mol compared to the educt. Hence, the difference in total dispersion energy contributes only marginally to the overall change in the energetics of this reaction step.

The correlation between dispersion interactions and structural changes becomes apparent when the dispersion contributions for reference structures and structures optimized with dispersion interactions are compared (see Table 1). The gain in dispersion energy is −11.9 kcal/mol for intermediate **4**, −3.4 kcal/mol for $\mathbf{TS}_{4,5}$ and −4.8 kcal/mol for intermediate **5**.

Table 1. Contributions to the Interaction Energies from the Dispersion Interaction between and within the Two Regions of Structures 4, $\mathbf{TS}_{4,5}$ and 5 (Compare Figure 3) in kcal/mol[a]

interaction	intermediate regions	BP86-D3	BP86-D3 ref struc.	TPSS-D3	TPSS-D3 ref struc.
4	1−1	−26.6	−26.2	−19.5	−19.2
4	1−2	−22.4	−11.1	−14.3	−9.1
4	2−2	−32.0	−31.7	−23.6	−23.4
4	total	−81.0	−69.1	−57.3	−51.7
$\mathbf{TS}_{4,5}$	1−1	−24.9	−24.7	−18.2	−18.0
$\mathbf{TS}_{4,5}$	1−2	−22.0	−19.1	−17.2	−15.0
$\mathbf{TS}_{4,5}$	2−2	−33.3	−33.1	−24.5	−24.4
$\mathbf{TS}_{4,5}$	total	−80.3	−76.9	−59.9	−57.4
5	1−1	−26.4	−26.0	−19.2	−19.0
5	1−2	−23.3	−19.0	−18.0	−15.0
5	2−2	−33.3	−33.0	−24.5	−24.3
5	total	−82.9	−78.1	−61.7	−58.3

[a]The values in the fourth and sixth column were calculated with the TPSS reference structures from Yang and Hall (ref struc.).

These gains in energy are dominated by the dispersion interactions between MPT^+ and FeGP.

As mentioned in the introduction, a hydride atom is transferred stereospecifically to the *pro-R* position of MPT^+.[10] Yang and Hall, however, considered hydride transfer to the *pro-S* position of MPT^+. Therefore, we analyzed changes in reaction energy and barrier height with respect to cosubstrate orientation. Interestingly, for rotated MPT^+ as shown in Figure 6 we obtain an endothermic reaction of 3.7 kcal/mol as

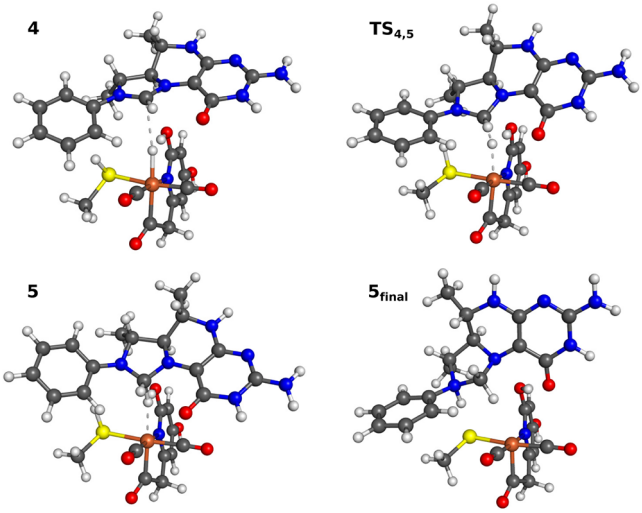

Figure 6. Structures of the hydride transfer step (**4** → **5**) with rotated MPT^+ (hydride transferred to the *pro-R* position). Structure **5** features one imaginary frequency (17i cm^{-1}). Further optimization leads to $\mathbf{5}_{final}$.

compared to 2.7 kcal/mol. The barrier height changes from 5.2 to 6.1 kcal/mol. Consequently, the energetics of this reaction step is not significantly changed and the conclusions therefore remain the same. Our results are corroborated by comparing with the experimentally determined kinetic isotope effect on the reverse reaction of [Fe] hydrogenase (i.e., H_2 formation). Estimating the kinetic isotope effect[57,58] from the C14a−H stretch frequency of 1668 cm^{-1} for intermediate **5** yields a value of 3.2 that compares well with the experimentally determined range of 2−3.[7] Hence the coordination of HMPT to the iron center substantially weakens the C14a−H bond.

For the cleavage of H_2 (**6** → **7**, **2**), we find that intermediate **2** is more stable than intermediate **7** in contrast to Yang and Hall's result, which was confirmed by recalculating the results with TPSS/6-31++g(d,p) and the IEFPCM as implemented in Gaussian03.[59] Furthermore step **7** → **3** has a low barrier of only +0.3 kcal/mol and step **2** → **3** has a barrier of +4.7 kcal/mol.

Our results lead to a modified interpretation of the reaction mechanism. The hydride transfer step is feasible and fast. H_2 cleavage is dependent on where deprotonation occurs. There are two possible pathways. It is energetically favorable to deprotonate at the sulfur atom of the cysteine ligand. However, the barrier for H_2 cleavage with H^+ transfer to the resulting cysteinate of 6.4 kcal/mol is significantly higher for this pathway. For model complexes it has recently been shown that protonation/deprotonation of a thiol ligand can in principle occur.[30,34] Moreover, in the crystal structure of [Fe] hydrogenase from *M. jannaschii* (PDB code: 3F47[37]) there is a lysine (Lys_{151}) in close proximity to the sulfur atom which could serve as a base for the cysteine proton. Deprotonation at the hydroxyl

dx.doi.org/10.1021/jp312662y | J. Phys. Chem. B 2013, 117, 4806−4817

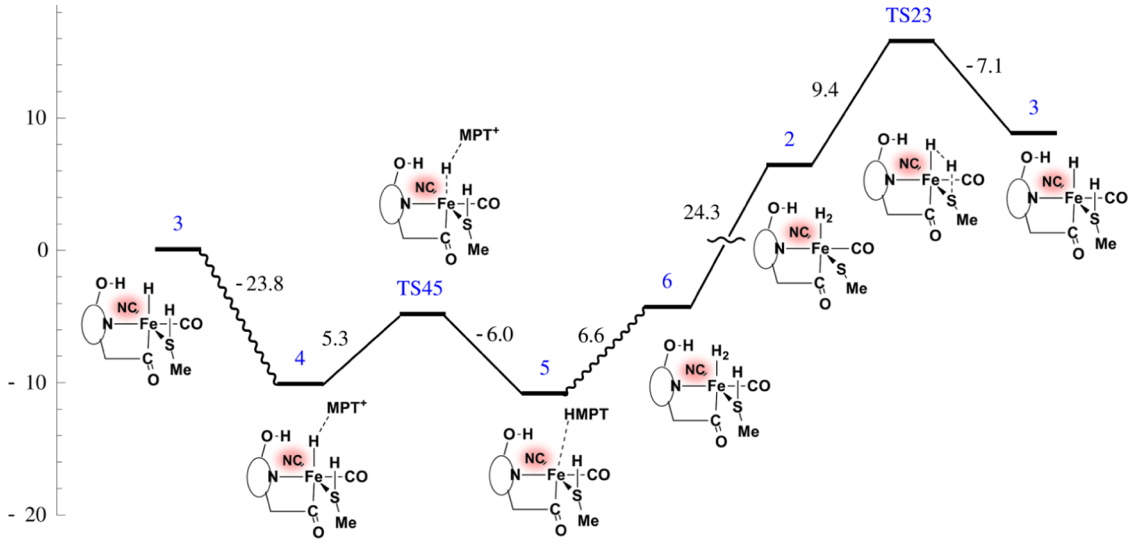

Figure 7. Free-energy profile for $[Fe]^{CN^-}$ calculated with BP86-D3/TZVP/COSMO (ε = 4). Gibbs free-energy differences are given in kcal/mol (T = 298 K, p = 1.013 bar).

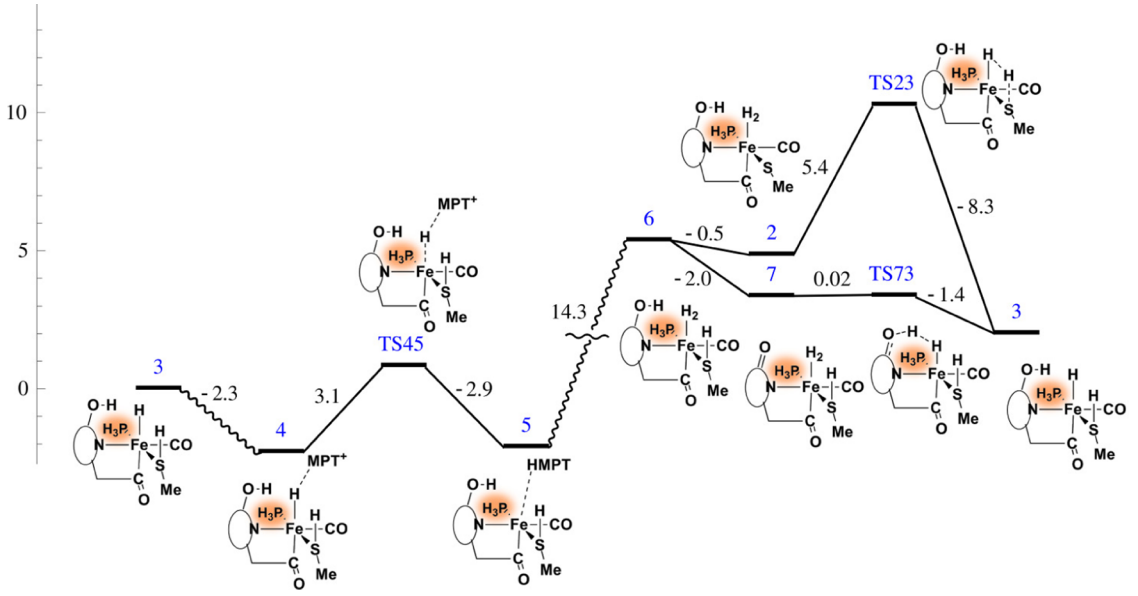

Figure 8. Free-energy profile for $[Fe]^{PH_3}$ calculated with BP86/TZVP/COSMO (ε = 4). Gibbs free-energy differences are given in kcal/mol (T = 298 K, p = 1.013 bar).

group of the pyridinol ligand is only slightly disfavored by 1.2 kcal/mol and H_2 cleavage with H^+ transfer to the hydroxyl anion is nearly barrier less. If deprotonation of the hydroxyl group occurs, H_2 cleavage will therefore be extremely fast. Support for the deprotonation of this hydroxyl group is provided by the observation that mutation of His_{14} to alanine results in a significantly reduced enzymatic activity of only 1% of the wild-type level.[36] In the crystal structure this residue is in close proximity to the hydroxyl group of the pyridinol ligand and could act as a base, thereby facilitating deprotonation. For existing iron complexes, related to [Fe] hydrogenase's active site, it is proposed that hydrogen is split heterolytically after coordination. The hydride remains at the metal center and the proton is transferred to the oxygen atom of a cyclopentadienon ligand, forming a hydroxyl group.[60] These complexes are stable and active as hydrogenation catalysts.[61,62]

3.2. Catalytic Cycle with Replaced Ligands.

3.2.1. $[Fe]^{CN^-}$. Having established the reaction profile with dispersion corrections for the wild type we can now compare to the variants with first-shell ligand substitutions. Especially the two main steps, hydride transfer and H_2 cleavage, are best suited for comparison. Moreover, they do not involve a change of reactant number. The free-energy profile (BP86-D3) for $[Fe]^{CN^-}$ is given in Figure 7. Surprisingly, the hydride transfer step (**4** → **5**) is exergonic by −0.7 kcal/mol with the negatively charged cyanide ligand in position 4. The reaction barrier is comparable to that of the wild type (+5.3 kcal/mol), hence the reaction will be fast at room temperature. The most important change compared with the native active-site model is that ΔG of the hydride transfer step changes its sign from an endergonic reaction to a slightly exergonic reaction. After dissociation of HMPT and coordination of the next H_2 molecule, the

dx.doi.org/10.1021/jp312662y | J. Phys. Chem. B 2013, 117, 4806−4817

deprotonation is highly endergonic (+24.3 kcal/mol). The neutral $[Fe]^{CN^-}$ complex is less likely to be deprotonated than the positively charged [Fe] complex, which is neutral after deprotonation. Nevertheless, the change from a slightly exergonic reaction to a strongly endergonic reaction favors the interpretation that the acidity of intermediate **3** is decreased and the acid−base equilibrium is shifted compared to [Fe]. Notably, no structure could be identified which would correspond to intermediate **7** of the original mechanism (see Figure 4) for it does not represent a minimum on the potential energy surface. Rather, structure optimization directly converges to intermediate **3**, indicating its spontaneous formation after deprotonation at the hydroxyl group. Reaction **2** → **3** is endergonic by +2.3 kcal/mol. Therefore, also for this step we observe a change in sign of ΔG compared to the original situation. Moreover, the barrier is significantly higher than that for the wild type's reaction (+9.4 kcal/mol compared to +4.7 kcal/mol). In summary, both steps which are suitable for comparison are inverted when changing CO to CN^- in terms of free energy. As a consequence the relative rates of forward an backward reaction for these elementary steps change.

3.2.2. [Fe]^{PH_3}. The free-energy profile for $[Fe]^{PH_3}$'s catalytic cycle is presented in Figure 8. The hydride transfer step **4** → **5** is almost thermoneutral (ΔG = +0.2 kcal/mol) and has a small barrier of +3.1 kcal/mol. The deprotonation is slightly exergonic. Notably, deprotonation of the hydroxyl group is favored by +1.5 kcal/mol, as opposed to [Fe], where deprotonation at the cysteine is slightly favored. The H_2 cleavage step (**7** → **3** or **2** → **3**) is exergonic, as for the wild type, but the difference in free energy is reduced in magnitude. Analogous to [Fe] the reaction **7** → **3** is nearly barrier less ($\Delta G^{\ddagger}$ = 0.02 kcal/mol), the change in free energy is −1.4 kcal/mol. If the hydroxyl group is deprotonated, H_2 cleavage is spontaneous. The barrier for H_2 cleavage with proton transfer to the thiolate is +5.4 kcal/mol, which is of the same magnitude as for [Fe], and the reaction is exergonic by −3.1 kcal/mol. The resulting picture for the whole cycle is similar to that of the wild type. If the hydroxyl group gets deprotonated, H_2 cleavage is straightforward. If the thiol gets deprotonated, H_2 cleavage has a considerable but still surmountable barrier. Nevertheless, it is important to note that the sign of ΔG for H_2 cleavage and hydride transfer does not change compared to [Fe] but the absolute values are smaller. Hydride transfer can be considered thermoneutral.

3.2.3. Effect of Ligand Exchanges. First of all, the fact that all ligand substitutions considered generate active-site variants that should be able to catalyze the given reaction is an interesting result that is not self-evident. However, the free-energy profiles of $[Fe]^{CN^-}$ and $[Fe]^{PH_3}$ demonstrate that the ligand in position 4 does affect the reactivity of the active site. The reaction steps which are best suited for comparison, i.e., hydride transfer and H_2 cleavage, are reversed by the changes introduced.

The negatively charged cyanide ligand, which is isoelectronic to CO and considered a less strong π-acceptor but better σ-donor than CO, renders the Fe center more reductive. The higher reductivity eases hydride transfer (**4** → **5**) because the leftover positive charge, when H^- is removed, is better compensated by cyanide. H_2 cleavage (**2** → **3**) is hindered by cyanide because the emerging negative charge of the hydride species is less well stabilized.

The energetics obtained for $[Fe]^{PH_3}$ are exactly in between those for [Fe] and $[Fe]^{CN^-}$. Step **4** → **5** is thermoneutral, the deprotonation is less exergonic than for [Fe] and step **7**,**2** → **3** is not inverted but its exergodicity is reduced. The σ-donor PH_3 pushes electrons to the iron center and thus has an effect comparable to cyanide. However, with PH_3 in position 4 two σ-donor ligands are in trans position with respect to each other which can be expected to be unfavorable. This underlines the exceptional role of cyanides in the active site of [FeFe] hydrogenases because these π-acceptors are still strong σ-donors. To mimic electronic characteristics of [FeFe] hydrogenase's active site an adequate replacement for the cyanides is thus necessary. Our results indicate that the donor strength of phosphines is still too weak to resemble that of cyanides which is in accordance with a recent QM/MM study of [FeFe] hydrogenases.[63] On the other hand, they may give general hints for the synthesis of monoiron model compounds with catalytic capabilities for H_2 splitting or proton reduction.

3.3. Kinetic Model for the H_2 Splitting Reaction. The complete catalytic cycle of [Fe] hydrogenase involves complicated dynamics of the enzyme and cofactor, which makes it difficult to predict the effect of changes in barrier heights and intermediate energies on the overall enzymatic turnover. In order to facilitate the comparison between active-site variants a simplified kinetic model of the complete pathway is desirable. Because the binding energies of MPT^+ and HMPT are not accessible within our theoretical description we reduce the complexity of the full cycle to a model comprising three essential reaction steps. These are H_2 coordination, H_2 splitting, and heterolytic dissociation of H^- and H^+ from the metal center

$$H_2 + M \underset{k_1^-}{\overset{k_1^+}{\rightleftharpoons}} M-H_2 \underset{k_2^-}{\overset{k_2^+}{\rightleftharpoons}} H-M-H \underset{k_3^-}{\overset{k_3^+}{\rightleftharpoons}} M + H^+ + H^- \quad \text{(R1)}$$

It should be emphasized that this model is a toy model to understand the effect of relative intermediate free energies on the total catalytic cycle and should not be understood as a realistic description for the [Fe] hydrogenase reaction. However, the general structure of the model will facilitate the comparison to synthetic H_2-splitting catalysts.

3.3.1. Steady-State Model of the Reaction. The time evolution of the concentrations of model reaction R1 can be described by a system of ordinary differential equations. This system can be solved analytically when the quasi-steady-state approximation is applied,[64] which implies constant intermediate concentrations. The resulting equations can be expressed in terms of these concentrations which we assume to be normalized, according to

$$\theta_M + \theta_{M-H_2} + \theta_{H-M-H} = 1 \quad (1)$$

The steady-state equations for the intermediates then read

$$\frac{d\theta_M}{dt} = k_1^-\theta_{M-H_2} + k_3^+\theta_{H-M-H} - k_1^+c_{H_2}\theta_M - k_3^-\theta_M c_{H^+}c_{H^-} = 0 \quad (2)$$

$$\frac{d\theta_{M-H_2}}{dt} = k_1^+\theta_M c_{H_2} + k_2^-\theta_{H-M-H} - k_1^-\theta_{M-H_2} - k_2^+\theta_{M-H_2} = 0 \quad (3)$$

dx.doi.org/10.1021/jp312662y | J. Phys. Chem. B 2013, 117, 4806−4817

$$\frac{d\theta_{H-M-H}}{dt} = k_2^+\theta_{M-H_2} + k_3^-\theta_M c_{H^+}c_{H^-} - k_3^+\theta_{H-M-H} - k_2^-\theta_{H-M-H} = 0 \quad (4)$$

The rate constants of these equations can be calculated from standard transition state theory[65,66]

$$k = \frac{k_B T}{h}\exp\left(\frac{-\Delta G^{\ddagger}}{RT}\right) \quad (5)$$

Here k_B is the Boltzmann constant, h the Planck constant, R the ideal gas constant, T the absolute temperature, and $\Delta G^{\ddagger}$ the free-energy barrier of the reaction step associated with the rate constant.

As discussed in section 3.1 the catalytic mechanism theoretically derived for [Fe] hydrogenase features two possible pathways for the H_2 cleavage step (via intermediate **2** or intermediate **7**) which are here examined separately. For the first pathway (pathway 1), where deprotonation occurs at the cystein's sulfur atom, the $\Delta G^{\ddagger}$ for the hydride transfer and the H_2 cleavage step (steps 2 and 3 in reaction R1) are taken from the calculated values of the catalytic cycle (compare Figures 5, 7, and 8).

For the H_2 coordination an assumption has to be made. The free-energy difference ΔG of this reaction step is adjusted so that the total free-energy difference ΔG_{tot} of the overall reaction is −1.3 kcal/mol, which is the reported ΔG_{tot} of the overall reaction catalyzed by [Fe] hydrogenase.[12] In order to avoid H_2 coordination to become the rate determining step we arbitrarily set the barrier to 1.0 kcal/mol for the exergonic reaction direction (note that the energetically preferred direction may vary depending on the chemical nature of the catalyst).

In the second pathway (pathway 2), the pyridinol's hydroxyl group is deprotonated. This causes an additional problem because intermediates **2** and **7** do not have the same energy (see e.g. Figure 5), meaning that ΔG of the H_2 cleavage step is different for both pathways. This cannot be reflected by the model reaction treated here. To circumvent this problem $\Delta G^{\ddagger}_{2,-}$ for the second pathway is adjusted so that ΔG_{tot} of the overall reaction is −1.3 kcal/mol for the variants considered. Therefore, k_2^- is increased for [Fe] and decreased for $[Fe]^{PH_3}$. It will be pointed out later why this does not affect the interpretation.

As discussed in section 3.2.1, there exists no stable intermediate **2** for $[Fe]^{CN^-}$ and deprotonation at the hydroxyl group of the pyridinol ligand would directly yield product **3**. This step cannot be described within our kinetic model. However, to resemble a situation as encountered for the first pathway, i.e. a change in sign of ΔG compared to the wild type, this step is constructed on purpose to have the same endergonic ΔG as for the first pathway (deprotonation at Cys-S). The barrier is set to 0.1 kcal/mol, in the exergonic reaction direction, to describe an almost spontaneous reaction.

This approach results in a consistent modeling of the second reaction pathway for all three variants and incorporates the change in sign of ΔG for both, hydride transfer and H_2 cleavage, as key feature of $[Fe]^{CN^-}$. Summarized, the second pathway is treated analogously to the first pathway in terms of free-energy differences but with a lower barrier for the H_2 cleavage step which can consistently be represented in the simplified model mechanism. It should be emphasized that this model gives insights what effects the change in the catalyst's ligand shell may afford. The resulting $\Delta G^{\ddagger}$ are listed in Table 2.

Table 2. $\Delta G^{\ddagger}$ for the Forward and Backward Elementary Reactions in Reaction R1 in kcal/mol[a]

reaction	[Fe]	$[Fe]^{CN^-}$	$[Fe]^{PH_3}$	[Fe]	$[Fe]^{CN^-}$	$[Fe]^{PH_3}$
$\Delta G^{\ddagger}_{1,+}$	1.0	1.0	2.4	1.0	1.0	2.4
$\Delta G^{\ddagger}_{1,-}$	1.4	3.9	1.0	1.4	3.9	1.0
$\Delta G^{\ddagger}_{2,-}$	4.7	9.4	5.4	0.3	2.4	0.1
$\Delta G^{\ddagger}_{2,-}$	8.3	7.1	8.3	3.9	0.1	3.0
$\Delta G^{\ddagger}_{3,-}$	5.2	5.3	3.1	5.2	5.3	3.1
$\Delta G^{\ddagger}_{3,-}$	2.5	6.0	2.9	2.5	6.0	2.9

[a]Columns two, three, and four present free-energy differences for the reaction pathways via deprotonation at the cysteine and the right most three columns for the pathway via deprotonation at the pyridinol's hydroxyl group. The subscripts "+" and "−" denote the forward and the backward reactions, respectively.

The steady-state rate eqs 2−4 can be solved with the help of graph theory.[64] With the definition of the equilibrium constant

$$K_{eq} = \frac{c^{eq}_{H^+}c^{eq}_{H^-}}{c^{eq}_{H_2}} = \frac{k^+}{k^-} = \frac{k_1^+k_2^+k_3^+}{k_1^-k_2^-k_3^-} \quad (6)$$

the rate can be written as

$$r = \frac{\left(c_{H_2} - \frac{c_{H^+}c_{H^-}}{K_{eq}}\right)}{\overline{k}_1 c_{H_2} + \overline{k}_2 c_{H^+}c_{H^-} + \overline{k}_3} \quad (7)$$

where

$$\overline{k}_1 = \frac{1}{k_3^+} + \frac{1}{k_2^+} + \frac{k_2^-}{k_2^+k_3^+} \quad (8)$$

$$\overline{k}_2 = \frac{k_1^-k_3^-}{k_1^+k_2^+k_3^+} + \frac{k_2^-k_3^-}{k_1^+k_2^+k_3^+} + \frac{k_3^-}{k_1^+k_3^+} \quad (9)$$

$$\overline{k}_3 = \frac{1}{k_1^+} + \frac{k_1^-k_2^-}{k_1^+k_2^+k_3^+} + \frac{k_1^-}{k_1^+k_2^+} \quad (10)$$

The numerator of eq 7 can be understood as thermodynamic driving force (deviation from equilibrium). The denominator can be understood as kinetic resistance Ω_{kin} in analogy to electricity.[67,68] The smaller Ω_{kin}, the faster the reaction. The kinetic resistances for both possible pathways (via intermediates **2** and **7** respectively) of the three catalytic cycles (for [Fe], $[Fe]^{CN^-}$, and $[Fe]^{PH_3}$, compare Figures 5, 7, and 8) are given in Table 3. It can be seen that for reaction pathway 1 the $[Fe]^{CN^-}$ variant is a worse catalyst than the wild type, which is the best. This is due to the higher barrier of the H_2 cleavage reaction. The rate constants k_2^+ and k_2^- are much smaller than the other rate constants.

For the second pathway, the kinetic resistances are smaller than for the first, especially for $[Fe]^{CN^-}$ and $[Fe]^{PH_3}$ (see Table 3). $[Fe]^{CN^-}$ has a kinetic resistance comparable to [Fe]. $[Fe]^{PH_3}$ has the lowest resistance and thus is the best catalyst. For the second reaction pathway the kinetic resistances are not determined by a single high barrier (as for the first pathway), so the contributions to the kinetic resistances are analyzed in detail to find out which step is dominating the kinetic resistance for each catalyst. The results are shown in Table 4.

dx.doi.org/10.1021/jp312662y | J. Phys. Chem. B 2013, 117, 4806−4817

Table 3. Kinetic Resistance Ω_{kin} (Denominator of eq 7) Evaluated for the Three Catalytic Cycles with the Concentration of Products and Educts Is Set to One ($c_{H_2} = c_{H^+} = c_{H^-} = 1$)[a]

variant	[Fe]	$[Fe]^{CN^-}$	$[Fe]^{PH_3}$
$\Omega_{kin,pathway1}$	2.376×10^{-8}	1.338×10^{-6}	3.911×10^{-8}
variant	[Fe]	$[Fe]^{CN^-}$	$[Fe]^{PH_3}$
$\Omega_{kin,pathway2}$	1.151×10^{-9}	6.215×10^{-8}	6.029×10^{-11}

[a]Upper half: reaction pathway 1 (deprotonation at cysteine). Lower half: reaction pathway 2 (deprotonation at the pyridinol's hydroxyl group).

Table 4. (Upper Part) Terms of the Kinetic Resistance Ω_{kin} for the [Fe], $[Fe]^{CN^-}$ and $[Fe]^{PH_3}$ Variants and (Lower Part) Terms Summing up to $\overline{k}_1$

	[Fe]	$[Fe]^{CN^-}$	$[Fe]^{PH_3}$
$\overline{k}_1$	1.052×10^{-9}	6.169×10^{-8}	3.066×10^{-11}
$\overline{k}_2$	9.649×10^{-11}	1.328×10^{-11}	1.594×10^{-11}
$\overline{k}_3$	2.229×10^{-12}	4.519×10^{-10}	1.370×10^{-11}
$1/k_3^+$	1.049×10^{-9}	1.242×10^{-9}	3.024×10^{-11}
$1/k_2^+$	2.672×10^{-13}	9.271×10^{-12}	1.906×10^{-13}
$k_2^-/(k_2^+k_3^+)$	2.401×10^{-12}	6.044×10^{-8}	2.257×10^{-13}

It can be seen that in all three cases $\overline{k}_1$ represents the largest contribution to the kinetic resistance. Analyzing the components of $\overline{k}_1$ tells which rate constants, and thereby which step, is dominating the kinetic resistance. The decomposition of $\overline{k}_1$ (eq 8) into its summands is presented in Table 4 (lower part). For the wild type and $[Fe]^{PH_3}$ the term $1/k_3^+$ is the largest. Hence, the endergonic hydride transfer is the rate limiting step for H_2 cleavage.

For $[Fe]^{CN^-}$ the term $k_2^-/(k_2^+k_3^+)$ is the largest. This is because k_2^- is larger for the $[Fe]^{CN^-}$ variant in comparison to the wild type and $[Fe]^{PH_3}$. This can be understood by looking at the catalytic profile presented in Figure 9. The reaction associated to k_2^- is the back reaction of H_2 cleavage, i.e., H_2 formation. Because the relative stability of intermediates M−H_2 and H−M−H changes upon ligand exchange, k_2^- is larger for $[Fe]^{CN^-}$ compared to [Fe] and $[Fe]^{PH_3}$. This can also be rationalized by considering intermediate M-H_2 to be a sink of the catalytic profile of $[Fe]^{CN^-}$, whereas for [Fe] and $[Fe]^{PH_3}$ the sink would be intermediate H−M−H. Apparently, the rate determining step is shifted from hydride transfer to H_2 cleavage by changing the catalysts' ligand from CO/PH_3 to CN^-.

Importantly, the reason for the different rate determining steps and kinetic resistances is the change in relative free energies and not the change in barrier heights between the different variants. The model reaction for $[Fe]^{CN^-}$ is, however, slower than that for [Fe] because not only the endergonic hydride transfer becomes exergonic but also the exergonic H_2 splitting becomes endergonic (by construction). One step becomes faster and the other slower, so the net effect is not an increased reaction rate. $[Fe]^{PH_3}$ has the energy profile with the smallest changes in free energy between the intermediates and also no large barrier over the whole reaction pathway. Consequently, $[Fe]^{PH_3}$ is the best catalyst.

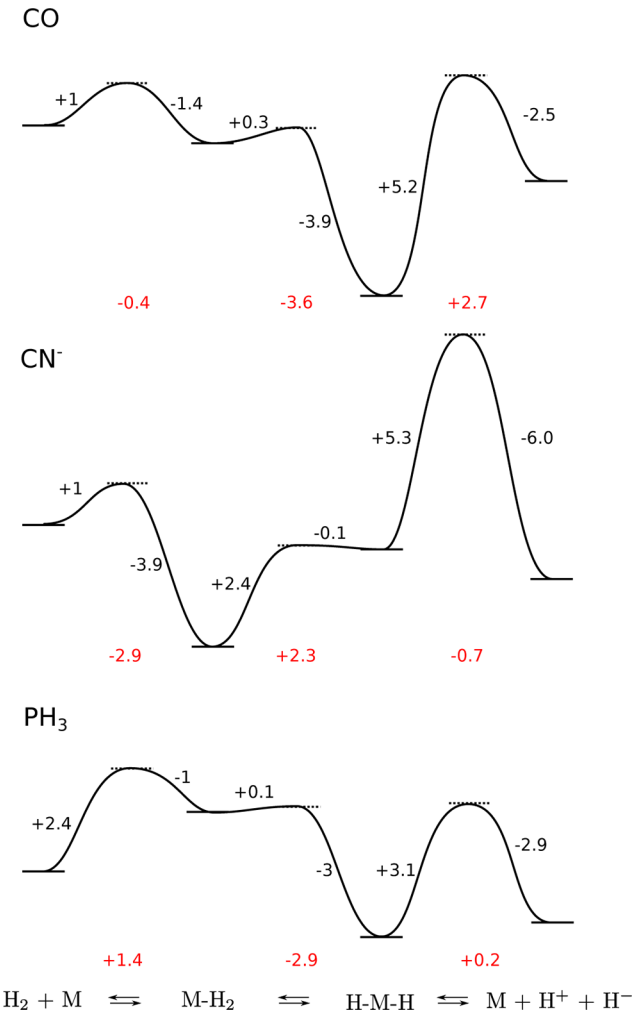

Figure 9. Energy profiles of the model mechanism set up for [Fe], $[Fe]^{CN^-}$, and $[Fe]^{PH_3}$. Energies are given in kcal/mol.

The change of the k_2^- constants for the second pathway did not affect these conclusions. For [Fe] k_2^- was increased, but the term $k_2^-/(k_2^+k_3^+)$ still is much smaller than the term $1/k_3^+$. For $[Fe]^{PH_3}$ k_2^- was decreased by a factor of 15. An increase by a factor of 15 would not make the term $k_2^-/(k_2^+k_3^+)$ dominant.

3.3.2. Irreversibility Assumption for Certain Reaction Steps. For the reaction catalyzed by [Fe] hydrogenase the following assumption can be made. The hydride transfer is accompanied by MPT^+ coordination and HMPT dissociation, a process which may be controlled by conformational changes of the enzyme (compare open and closed conformation of the enzyme[56]). One could interpret the change from the open to the closed conformation and the concomitant removal of the hydride acceptor as a process which makes the hydride transfer irreversible, because HMPT is removed from the active site after H^- transfer. In the minimal model, this can be described by assuming that the last step is irreversible and therefore k_3^- is zero. The resulting rate equation can be written as

$$r = c_{H_2}\left(c_{H_2}\left(\frac{1}{k_3^+} + \frac{1}{k_2^+} + \frac{k_2^-}{k_2^+k_3^+}\right) + \frac{1}{k_1^+} + \frac{k_1^-k_2^-}{k_1^+k_2^+k_3^+} + \frac{k_1^-}{k_1^+k_2^+}\right)^{-1} \quad (11)$$

dx.doi.org/10.1021/jp312662y | J. Phys. Chem. B 2013, 117, 4806−4817

Again the denominator can be interpreted as kinetic resistance Ω_{kin} where we can identify

$$\overline{k}_1 = \frac{1}{k_3^+} + \frac{1}{k_2^+} + \frac{k_2^-}{k_2^+ k_3^+} \quad (12)$$

$$\overline{k}_3 = \frac{1}{k_1^+} + \frac{k_1^- k_2^-}{k_1^+ k_2^+ k_3^+} + \frac{k_1^-}{k_1^+ k_2^+} \quad (13)$$

as for the full rate equations (see eqs 8 and 10). $\overline{k}_2$ (eq 9) equals zero and drops out. It can be seen that the resistance does not depend on the product concentrations anymore because the product formation is irreversible now. However, comparison with Table 4 shows that in all cases $\overline{k}_1$ was the largest term in the kinetic resistance (neglecting the multiplication with the concentrations) which means that the reaction rate under steady-state conditions is slightly enhanced. However, now the system is in a nonequilibrium state and the driving force is only given by the educt concentration. So it can be concluded that the irreversible step does not significantly accelerate the reaction but there are no "thermodynamic constraints" anymore. The reaction flow is then in the product direction. This description corresponds to the assumption that the catalyzed reaction is modeled for an open system.

4. CONCLUSION

The special coordination chemistry observed in the active site of [Fe] hydrogenases raises the question about the necessity of the particular ligand choices for the catalysis of heterolytic H_2 cleavage. Remarkably, we find that the established reaction mechanism is compatible with the rather severe ligand substitutions considered in this work. Apart from differences in the overall reaction rates all variants should facilitate H_2 splitting based on the kinetic and thermodynamic data determined. The regular catalytic pathway of the unmodified [Fe] hydrogenase active-site model features a rather flat energy profile as shown in section 3.1 which explains its high activity. By comparing with the findings of Yang and Hall[39] we conclude that a less endergonic hydride transfer reaction is obtained when dispersion interactions between the cosubstrate MPT^+ and FeGP are considered explicitly in the calculations. With the resulting lower barrier hydride transfer cannot be considered the rate determining step anymore. The study of active-site variants presented in this work has shown that the features of the catalytic energy profile are strongly affected by ligand substitutions in the first coordination sphere of the active Fe atom of FeGP which, like in the case of $[Fe]^{CN^-}$, may even inverse the energetics of single elementary reactions, i.e., H_2 splitting and H^- transfer. In this context it is important to remember that the CO by CN^- substitution results in a ligand arrangement that resembles that found in [FeFe] hydrogenase. As we have seen a simplified kinetic model of the catalytic process under consideration can significantly facilitate the interpretation of results. By this means, we are able to identify general features of the [Fe] hydrogenase's active site being important for the high catalytic activity. Depending on the pathway for H_2 cleavage we find that the barrier height of a single elementary reaction can significantly diminish catalytic activity like in the case of $[Fe]^{CN^-}$. Here, the CN^- ligand in position four renders heterolytic H_2 cleavage less favorable. In contrast, both [Fe] and $[Fe]^{PH_3}$ feature only moderate barriers and are therefore more active catalysts, which also explains the ligand choice of CO in naturally occurring [Fe] hydrogenases. Based on the kinetic analysis it turns out that $[Fe]^{PH_3}$ should outperform the native [Fe] form. However, two trans donor ligands, as in $[Fe]^{PH_3}$, might be difficult to realize in model compounds. Regarding the ambiguity of the H_2 splitting step we found deprotonation via the hydroxyl group of the pyridinol ligand to be the kinetically favored pathway for all three active-site variants considered. It is therefore likely that the cysteine sulfur atom remains deprotonated throughout catalysis. In this case kinetic efficiency is determined by the free energies of all intermediates involved. Active-site variants that do not feature energetic sinks in their energy profile, as it is the case for, e.g., $[Fe]^{CN^-}$, are therefore most active.

AUTHOR INFORMATION

Corresponding Author

*E-mail: markus.reiher@phys.chem.ethz.ch. Tel.: +41446334308.

Notes

The authors declare no competing financial interest.

ACKNOWLEDGMENTS

This work has been financially supported by ETH Zurich and the Schweizer Nationalfonds (Project No. 200021L_138536).

REFERENCES

(1) Vincent, K. A.; Parker, A.; Armstrong, F. A. Investigating and Exploiting the Electrocatalytic Properties of Hydrogenases. *Chem. Rev.* **2007**, *107*, 4366−4413.

(2) Fontecilla-Camps, J. C.; Volbeda, A.; Cavazza, C.; Nicolet, Y. Structure/Function Relationships of [NiFe]- and [FeFe]-Hydrogenases. *Chem. Rev.* **2007**, *107*, 4273−4303.

(3) Lubitz, W.; Reijerse, E.; van Gastel, M. [NiFe] and [FeFe] Hydrogenases Studied by Advanced Magnetic Resonance Techniques. *Chem. Rev.* **2007**, *107*, 4331−4365.

(4) Siegbahn, P. E. M.; Tye, J. W.; Hall, M. B. Computational Studies of [NiFe] and [FeFe] Hydrogenases. *Chem. Rev.* **2007**, *107*, 4414−4435.

(5) Ghirardi, M. L.; Posewitz, M. C.; Maness, P. C.; Dubini, A.; Yu, J.; Seibert, M. Hydrogenases and Hydrogen Photoproduction in Oxygenic Photosynthetic Organisms. *Annu. Rev. Plant Biol.* **2007**, *58*, 71−91.

(6) Schwörer, B.; Fernandez, V. M.; Zirngibl, C.; Thauer, R. K. H_2-Forming N^5,N^{10}-Methylenetetrahydromethanopterin Dehydrogenase from *Methanobacterium thermoautotrophicum*. *Eur. J. Biochem.* **1993**, *212*, 255−261.

(7) Klein, A. R.; Hartmann, G. C.; Thauer, R. K. Hydrogen Isotope Effects in the Reactions Catalyzed by H_2-Forming N^5,N^{10}-Methylenetetrahydromethanopterin Dehydrogenase from Methanogenic Archaea. *Eur. J. Biochem.* **1995**, *233*, 372−376.

(8) Hartmann, G. C.; Santamaria, E.; Fernández, V. M.; Thauer, R. K. Studies on the Catalytic Mechanism of H_2-Forming Methylenetetrahydromethanopterin Dehydrogenase: Para-Ortho H_2 conversion rates in H_2O and D_2O. *J. Biol. Inorg. Chem.* **1996**, *1*, 446−450.

(9) Zirngibl, C.; van Dongen, W.; Schwörer, B.; von Bünau, R.; Richter, M.; Klein, A.; Thauer, R. K. H_2-Forming Methylenetetrahydromethanopterin Dehydrogenase, a Novel Type of Hydrogenase without Iron-Sulfur Clusters in Methanogenic Archaea. *Eur. J. Biochem.* **1992**, *208*, 511−520.

(10) Schleucher, J.; Griesinger, C.; Schwoerer, B.; Thauer, R. K. H_2-Forming N^5,N^{10}-methylenetetrahydromethanopterin Dehydrogenase from *Methanobacterium thermoautotrophicum* Catalyzes a Stereoselective Hydride Transfer as Determined by Two-Dimensional NMR Spectroscopy. *Biochemistry* **1994**, *33*, 3986−3993.

(11) Schleucher, J.; Schwörer, B.; Thauer, R. K.; Griesinger, C. Elucidation of the Stereochemical Course of Chemical Reactions by Magnetic Labeling. *J. Am. Chem. Soc.* **1995**, *117*, 2941−2942.
(12) Thauer, R. K. Energy Metabolism of Methanogenic Bacteria. *Biochim. Biophys. Acta* **1990**, *1018*, 256−259.
(13) Stiebritz, M. T.; Reiher, M. Hydrogenases and Oxygen. *Chem. Sci.* **2012**, *3*, 1739−1751.
(14) Stiebritz, M. T.; Reiher, M. Theoretical Study of Dioxygen Induced Inhibition of [FeFe]-Hydrogenase. *Inorg. Chem.* **2009**, *48*, 7127−7140.
(15) Stiebritz, M. T.; Reiher, M. Corrections to Theoretical Study of Dioxygen Induced Inhibition of [FeFe]-Hydrogenase. *Inorg. Chem.* **2010**, *49*, 8645.
(16) Bruska, M. K.; Stiebritz, M. T.; Reiher, M. Regioselectivity of H Cluster Oxidation. *J. Am. Chem. Soc.* **2011**, *133*, 20588−20603.
(17) Bruska, M.; Stiebritz, M. T.; Reiher, M. Analysis of Differences in Oxygen Sensitivity of Fe-S Clusters. *Dalton Trans.* **2013**, DOI: 10.1039/C3DT50763G.
(18) Lyon, E. J.; Shima, S.; Buurman, G.; Chowdhuri, S.; Batschauer, A.; Steinbach, K.; Thauer, R. K. UV-A/Blue-Light Inactivation of the 'Metal-Free' Hydrogenase (Hmd) from Methanogenic Archaea. *Eur. J. Biochem.* **2004**, *271*, 195−204.
(19) Stiebritz, M. T.; Finkelmann, A. R.; Reiher, M. Oxygen Coordination to the Active Site of Hmd in Relation to [FeFe] Hydrogenase. *Eur. J. Inorg. Chem.* **2011**, *2011*, 1163−1171.
(20) Stiebritz, M. T.; Reiher, M. A Unifying Structural and Electronic Concept for Hmd and [FeFe] Hydrogenase Active Sites. *Inorg. Chem.* **2010**, *49*, 5818−5823.
(21) Tard, C.; Pickett, C. J. Structural and Functional Analogues of the Active Sites of the [Fe]-, [NiFe]-, and [FeFe]-Hydrogenase. *Chem. Rev.* **2009**, *109*, 2245−2274.
(22) Rakowski Dubois, M.; Dubois, D. L. Development of Molecular Electrocatalysts for CO_2 Reduction and H_2 Production/Oxidation. *Acc. Chem. Res.* **2009**, *42*, 1974−1982.
(23) Helm, M. L.; Stewart, M. P.; Bullock, R. M.; DuBois, M. R.; DuBois, D. L. A Synthetic Nickel Electrocatalyst with a Turnover Frequency Above 100,000 s^{-1} for H_2 Production. *Science* **2011**, *333*, 863−866.
(24) Wang, X.; Li, Z.; Zeng, X.; Luo, Q.; Evans, D. J.; Pickett, C. J.; Liu, X. The Iron Centre of the Cluster-Free Hydrogenase (Hmd): Low-Spin Fe(II) or Low-Spin Fe(0)? *Chem. Commun.* **2008**, *30*, 3555−3557.
(25) Li, B.; Liu, T.; Popescu, C. V.; Bilko, A.; Darensbourg, M. Y. Synthesis and Mössbauer Characterization of Octahedral Iron(II) Carbonyl Complexes $FeI_2(CO)_3L$ and $FeI_2(CO)_2L_2$: Developing Models of the [Fe]-H_2ase Active Site. *Inorg. Chem.* **2009**, *48*, 11283−11289.
(26) Royer, A. M.; Rauchfuss, T. B.; Gray, D. L. Oxidative Addition of Thioesters to Iron(0): Active-Site Models for Hmd, Nature's Third Hydrogenase. *Organometallics* **2009**, *28*, 3618−3620.
(27) Liu, T.; Li, B.; Popescu, C. V.; Bilko, A.; Pérez, L. M.; Hall, M. B.; Darensbourg, M. Y. Analysis of a Pentacoordinate Iron Dicarbonyl as Synthetic Analogue of the Hmd or Mono-Iron Hydrogenase Active Site. *Chem.—Eur. J.* **2010**, *16*, 3083−3089.
(28) Chen, D.; Scopelliti, R.; Hu, X. [Fe]-Hydrogenase Models Featuring Acylmethylpyridinyl Ligands. *Angew. Chem., Int. Ed.* **2010**, *49*, 7512−7515.
(29) Chen, D.; Scopelliti, R.; Hu, X. Synthesis and Reactivity of Iron Acyl Complexes Modeling the Active Site of [Fe]-Hydrogenase. *J. Am. Chem. Soc.* **2010**, *132*, 928−929.
(30) Royer, A. M.; Salomone-Stagni, M.; Rauchfuss, T. B.; Meyer-Klaucke, W. Iron Acyl Thiolato Carbonyls: Structural Models for the Active Site of the [Fe]-Hydrogenase (Hmd). *J. Am. Chem. Soc.* **2010**, *132*, 16997−17003.
(31) Chen, D.; Scopelliti, R.; Hu, X. A Five-Coordinate Iron Center in the Active Site of [Fe]-Hydrogenase: Hints from a Model Study. *Angew. Chem., Int. Ed.* **2011**, *50*, 5671−5673.
(32) Turrell, P. J.; Wright, J. A.; Peck, J. N. T.; Oganesyan, V. S.; Pickett, C. J. The Third Hydrogenase: A Ferracyclic Carbamoyl with Close Structural Analogy to the Active Site of Hmd. *Angew. Chem., Int. Ed.* **2010**, *49*, 7508−7511.
(33) Chen, D.; Ahrens-Botzong, A.; Schünemann, V.; Scopelliti, R.; Hu, X. Synthesis and Characterization of a Series of Model Complexes of the Active Site of [Fe]-Hydrogenase (Hmd). *Inorg. Chem* **2011**, *50*, 5249−5257.
(34) Chen, D.; Scopelliti, R.; Hu, X. Reversible Protonation of a Thiolate Ligand in an [Fe]-Hydrogenase Model Complex. *Angew. Chem.* **2012**, *51*, 1955−1957.
(35) Song, L.-C.; Xie, Z.-J.; Wang, M.-M.; Zhao, G.-Y.; Song, H.-B. Biomimetic Models for the Active Site of [Fe]Hydrogenase Featuring an Acylmethyl(hydroxymethyl)pyridine Ligand. *Inorg. Chem.* **2012**, *51*, 7466−7468.
(36) Shima, S.; Pilak, O.; Vogt, S.; Schick, M.; Stagni, M. S.; Meyer-Klaucke, W.; Warkentin, E.; Thauer, R. K.; Ermler, U. The Crystal Structure of [Fe]-Hydrogenase Reveals the Geometry of the Active Site. *Science* **2008**, *321*, 572−575.
(37) Hiromoto, T.; Ataka, K.; Pilak, O.; Vogt, S.; Stagni, M. S.; Meyer-Klaucke, W.; Warkentin, E.; Thauer, R. K.; Shima, S.; Ermler, U. The Crystal Structure of C176A Mutated [Fe]-Hydrogenase Suggests an Acyl-Iron Ligation in the Active Site Iron Complex. *FEBS Lett.* **2009**, *583*, 585−590.
(38) Liu, X.; Ibrahim, S. K.; Tard, C.; Pickett, C. J. Iron-Only Hydrogenase: Synthetic, Structural and Reactivity Studies of Model Compounds. *Coord. Chem. Rev.* **2005**, *249*, 1641−1652.
(39) Yang, X.; Hall, M. B. Monoiron Hydrogenase Catalysis: Hydrogen Activation with the Formation of a Dihydrogen, Fe−$H^{\delta-}\cdots H^{\delta+}$−O, Bond and Methenyl-$H_4MPT^+$ Triggered Hydride Transfer. *J. Am. Chem. Soc.* **2009**, *131*, 10901−10908.
(40) Perdew, J. P. Density-Functional Approximation for the Correlation Energy of the Inhomogeneous Electron Gas. *Phys. Rev. B* **1986**, *33*, 8822−8824.
(41) Becke, A. D. Density-Functional Exchange-Energy Approximation with Correct Asymptotic Behavior. *Phys. Rev. A* **1988**, *38*, 3098−3010.
(42) Tao, J.; Perdew, J. P.; Staroverov, V. N.; Scuseria, G. E. Climbing the Density Functional Ladder: Nonempirical Meta−Generalized Gradient Approximation Designed for Molecules and Solids. *Phys. Rev. Lett.* **2003**, *91*, 146401.
(43) Schäfer, A.; Huber, C.; Ahlrichs, R. Fully Optimized Contracted Gaussian Basis Sets of Triple Zeta Valence Quality for Atoms Li to Kr. *J. Chem. Phys.* **1994**, *100*, 5829−5835.
(44) Grimme, S.; Antony, J.; Ehrlich, S.; Krieg, H. A Consistent and Accurate *Ab Initio* Parametrization of Density Functional Dispersion Correction (DFT-D) for the 94 Elements H-Pu. *J. Chem. Phys.* **2010**, *132*, 154104.
(45) Ahlrichs, R.; Bär, M.; Häser, M.; Horn, H.; Kölmel, C. Electronic Structure Calculations on Workstation Computers: The Program System Turbomole. *Chem. Phys. Lett.* **1989**, *162*, 165−169.
(46) Eichkorn, K.; Weigend, F.; Treutler, O.; Ahlrichs, R. Auxiliary Basis Sets for Main Row Atoms and Transition Metals and Their Use to Approximate Coulomb Potentials. *Theor. Chem. Acc.* **1997**, *97*, 119−124.
(47) Klamt, A.; Schüürmann, G. COSMO: A New Approach to Dielectric Screening in Solvents with Explicit Expressions for the Screening Energy and its Gradient. *J. Chem. Soc. Perk. T. 2* **1993**, 799−805.
(48) Sillanpää, A. J.; Aksela, R.; Laasonen, K. Density Functional Complexation Study of Metal Ions with (Amino) Polycarboxylic Acid Ligands. *Phys. Chem. Chem. Phys.* **2003**, *5*, 3382−3393.
(49) Siegbahn, P. E. M.; Blomberg, M. R. A.; Pavlov, M. A Comparison of Electron Transfer in Ribonucleotide Reductase and the Bacterial Photosynthetic Reaction Center. *Chem. Phys. Lett.* **1998**, *292*, 421−430.
(50) Scott, A. P.; Radom, L. Harmonic Vibrational Frequencies: An Evaluation of Hartree-Fock, Møller-Plesset, Quadratic Configuration Interaction, Density Functional Theory, and Semiempirical Scale Factors. *J. Phys. Chem.* **1996**, *100*, 16502−16513.

(51) Reiher, M.; Hess, B. A. A Quantum-Chemical Study of Dinitrogen Reduction at Mononuclear Iron−Sulfur Complexes with Hints to the Mechanism of Nitrogenase. *Chem.—Eur. J* **2002**, *8*, 5332−5339.
(52) Tawa, G. J.; Topol, I. A.; Burt, S. K.; Caldwell, R. A.; Rashin, A. A. Calculation of the Aqueous Solvation Free Energy of the Proton. *J. Chem. Phys.* **1998**, *109*, 4852−4863.
(53) Klots, C. E. Solubility of Protons in Water. *J. Phys. Chem.* **1981**, *85*, 3585−3588.
(54) CHEMDRAW ULTRA 11.0; CambridgeSoft: Cambridge, MA, 2008.
(55) DeLano, W. L. *The PyMOL Molecular Graphics System*; DeLano Scientific: San Carlos, CA, 2002.
(56) Hiromoto, T.; Warkentin, E.; Moll, J.; Ermler, U.; Shima, S. The Crystal Structure of an [Fe]-Hydrogenase−Substrate Complex Reveals the Framework for H_2 Activation. *Angew. Chem., Int. Ed.* **2009**, *48*, 6457−6460.
(57) Antoniou, D.; Schwartz, S. D. Internal Enzyme Motions as a Source of Catalytic Activity: Rate-Promoting Vibrations and Hydrogen Tunneling. *J. Phys. Chem. B* **2001**, *105*, 5553−5558.
(58) Bell, R. P. *The Tunnel Effect in Chemistry*; Chapman and Hall: London, 1980.
(59) Frisch, M. J.; et al. *Gaussian 03*, revision E.01; Gaussian, Inc.: Wallingford, CT, 2004.
(60) von der Höh, A.; Berkessel, A. Insight into the Mechanism of Dihydrogen-Heterolysis at Cyclopentadienone Iron Complexes and Subsequent C═X Hydrogenation. *ChemCatChem* **2011**, *3*, 861−867.
(61) Knölker, H.-J.; Baum, E.; Goesmann, H.; Klauss, R. Demetalation of Tricarbonyl(cyclopentadienone)iron Complexes Initiated by a Ligand Exchange Reaction with NaOH−X-Ray Analysis of a Complex with Nearly Square-Planar Coordinated Sodium. *Angew. Chem., Int. Ed.* **1999**, *38*, 2064−2066.
(62) Casey, C. P.; Guan, H. An Efficient and Chemoselective Iron Catalyst for the Hydrogenation of Ketones. *J. Am. Chem. Soc.* **2007**, *129*, 5816−5817.
(63) Bruschi, M.; Greco, C.; Bertini, L.; Fantucci, P.; Ryde, U.; De Gioia, L. Functionally Relevant Interplay between the Fe_4S_4 Cluster and CN^- Ligands in the Active Site of [FeFe]-Hydrogenases. *J. Am. Chem. Soc.* **2010**, *132*, 4992−4993.
(64) Marin, G.; Yablonsky, G. *Kinetics of Chemical Reactions: Decoding Complexity*; Wiley-VCH: Weinheim, Germany, 2011.
(65) Eyring, H. The Activated Complex in Chemical Reactions. *J. Chem. Phys.* **1935**, *3*, 107−115.
(66) Laidler, K. J.; King, M. C. The Development of Transition-State Theory. *J. Phys. Chem.* **1983**, *87*, 2657−2664.
(67) Fishtik, I.; Callaghan, C. A.; Datta, R. Reaction Route Graphs. I. Theory and Algorithm. *J. Phys. Chem. B* **2004**, *108*, 5671−5682.
(68) Fishtik, I.; Callaghan, C. A.; Datta, R. Reaction Route Graphs. II. Examples of Enzyme-and Surface-Catalyzed Single Overall Reactions. *J. Phys. Chem. B* **2004**, *108*, 5683−5697.